Electronic and Geometric Properties of Au Nanoparticles on Highly Ordered Pyrolytic Graphite (HOPG) Studied Using X-ray Photoelectron Spectroscopy (XPS) and Scanning Tunneling Microscopy (STM)

Ignacio Lopez-Salido, Dong Chan Lim,* Rainer Dietsche, Nils Bertram, and Young Dok Kim*

Department of Physics, University of Konstanz, D-78457 Konstanz, Germany

Received: August 24, 2005; In Final Form: October 21, 2005

Au nanoparticles grown on mildly sputtered Highly Ordered Pyrolytic Graphite (HOPG) surfaces were studied using Scanning Tunneling Microscopy (STM) and X-ray Photoelectron Spectroscopy (XPS). The results were compared with those of Ag nanoparticles on the same substrate. By varying the defect densities of HOPG and the Au coverages, one can create Au nanoparticles in various sizes. At high Au coverages, the structures of the Au films significantly deviate from the ideal truncated octahedral form: the existence of many steps between different Au atomic layers can be observed, most likely due to a high activation barrier of the diffusion of Au atoms across the step edges. This implies that the particle growth at room temperature is strongly limited by kinetic factors. Hexagonal shapes of Au structures could be identified, indicating preferential growth of Au nanostructures along the (111) direction normal to the surface. In the case of Au, XPS studies reveal a weaker core level shift with decreasing particle size compared to the 3d level in similarly sized Ag particles. Also taking into account the Auger analysis of the Ag particles, the core level shifts of the metal nanoparticles on HOPG can be understood in terms of the metal/substrate charge transfer. Ag is (partially) positively charged, whereas Au negatively charged on HOPG. It is demonstrated that XPS can be a useful tool to study metal−support interactions, which plays an important role for heterogeneous catalysis, for example.

1. Introduction

The interest in the structures of nanoparticles has been increasing over the past few years due to their unexpected electronic, geometric, and chemical properties, which are of importance for both fundamental research as well as applications.[1−3] One of the widely used tools to characterize electronic structures of metal nanoparticles is photoemission spectroscopy, in particular X-ray Photoelectron Spectroscopy (XPS).[4−28] It has often been observed that a decrease of particle size causes a positive core level shift. In many cases, this behavior has been rationalized in terms of the inefficient screening of the final state of the photoemission process, in particular when metal particles are deposited on a poorly conducting substrate or when metal particles are surrounded by organic ligands.[4−13] Within this model, the core level shift is inversely proportional to the mean particle diameter. However, the importance of initial state effects has also been invoked: with decreasing particle size, the lattice strain increases, which may also induce positive core level shifts due to initial state effects.[14] Metal−insulator transitions can also be responsible for the positive core level shifts.[15] Furthermore, the charging of the metal nanoparticles (metal−support charge transfer) can yield the core level shifts.[16,17] The core level shifts may be influenced by the particle geometry, since different geometries yield change of the number of undercoordinated atoms, which have different electronic structures than bulk atoms.[18−22] Because of the numerous factors contributing to the core level shifts, the interpretation of XPS data of nanoparticles is sometimes not straightforward. The contribution of initial state effects observed for metal particles on oxide substrates is generally significantly smaller than that of final state effects.[4,8]

Highly Ordered Pyrolytic Graphite (HOPG) surfaces form very useful substrates for the growth of metal nanoparticles: due to the inert nature of this surface, the sample preparation is relatively easy. Moreover, oxygen chemisorption on metal nanoparticles can be well-studied using HOPG substrates, since there is no oxygen background signal.[29−31] In contrast, the use of oxide surfaces as substrates for the growth of nanoparticles results in the appearance of high O background signals in the spectroscopic studies (e.g., XPS), making investigations on oxygen chemisorption on metal nanoparticles difficult. A drawback of using HOPG is the very weak interaction between the metal particles and the substrate, which does not allow reliable Scanning Tunneling Microscopy (STM)/Atomic Force Microscopy (AFM) imaging of the nanoparticles due to the easy tip-induced movements of the particles. Recently, STM images of metal particles on HOPG surfaces have been taken after having defect sites on HOPG in order to stabilize the metal nanoparticles.[32,33] Much stronger interactions between defect sites of HOPG and metal with respect to the nondefect surfaces have been observed in the previous studies.

In the present work, we studied the growth of Au nanoparticles and nanostructured thin films on HOPG by means of STM. The preferential growth of Au along the (111) direction perpendicular to the surface is suggested, since the formation of the hexagonal Au planes was identified, indicating the formation of the (111) plane. No ideal truncated octahedral structures could be found, which has been observed in other previous studies for Au nanoparticles on other substrates or on HOPG with nanopits, but under different Au growth conditions from ours.[34,35] Instead, the existence of multiple steps between

* To whom the correspondence should be addressed. E-mails: dongchan.lim@uni-konstanz.de (for D.C.L.), young.kim@uni-konstanz.de (for Y.D.K.).

10.1021/jp054790g CCC: $33.50
Published on Web 12/16/2005

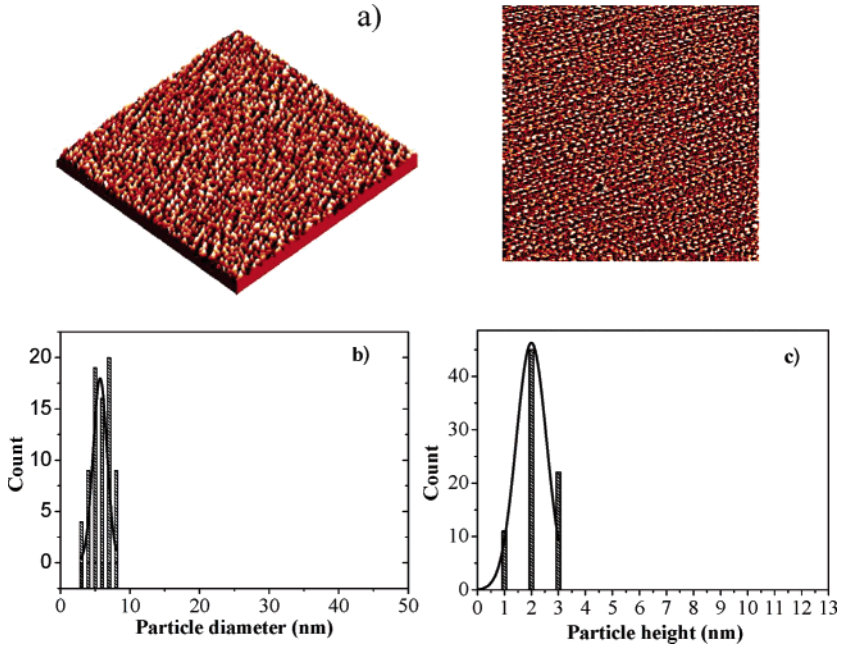

Figure 1. STM data of Au nanoparticles on HOPG are demonstrated. The HOPG sample was sputtered for 10 s (P(Ar) = 5×10^{-5} Torr, 0.5 kV), and Au was evaporated for 2 min with an emission current of 15 mA for evaporating. (a) A 2D and a 3D display of the same image, 300 m × 300 nm, tunneling parameter: −5.3 V, 0.08 nA. (b and c) Statistics of the particle diameters and heights.

different (111) planes could be observed, implying that the particle growth at room temperature can be kinetically hindered (Ehrlich−Schwoebel barrier).[36−38] XPS was used for the investigations of the electronic structures of Au nanoparticles, and the results of Au were compared with the previous studies on Ag on HOPG obtained in our group.[33] For Ag and Au, much different electronic behaviors have been observed. In combination with the Auger analysis of the Ag data, we suggest that the core level shifts of Ag and Au nanoparticles on HOPG are dominated by initial state effects. In this context, the charge transfer between metal particles and substrates has a large influence on the core level shifts. In our studies, Au and Ag particles on HOPG were prepared in the same way, and therefore, the results of Ag and Au can be directly compared. We show that the Auger analysis and the comparison of the core level shifts of various metal nanoparticles on the same substrate can shed light onto the origin of the core level shifts of nanoparticles.

2. Experimental Details

All experiments were performed under Ultrahigh Vacuum (UHV) conditions. Two different chambers were used for the STM and XPS studies. The first UHV chamber is equipped with an STM (OMICRON STM1), a Cylindrical Mirror Analyzer (CMA) for Auger Electron Spectroscopy (AES) measurements, a He UV lamp and a Low Energy Electron Diffraction system (LEED). A sputter-gun is installed for cleaning samples and creating defect sites in order to increase the sticking probabilities of the metals on HOPG surfaces (in this work, 0.5 kV Ar ions were used; the defect density was controlled by altering the sputtering time and the Ar pressure in the chamber).[39] The sample current during sputtering is typically 1 uA, while an Ar pressure of $\sim 2 \times 10^{-5}$ Torr was used. In this case, we estimate the rate of creating defects to be less than ∼0.5% of a monolayer per second. Note that a sputtering of 10 s did not show any C 1s peak broadening and decrease of the C plasmon peak, implying that the defect density in this case is below the XPS detection limit (∼5%). However, longer sputtering process (>20 s) leads to a broadening of the C 1s peak and a decrease of the C plasmon peak. The HOPG samples prepared by the scotch-tape pilling method were inserted into the UHV system and outgassed at about 1100 K. The cleanliness of HOPG was confirmed by means of STM and XPS (X-ray source: Al Kα, photon energy = 1486.6 eV). After this sample treatment, we could observe large terraces on the HOPG surface using STM, and the impurity level of the substrate determined by XPS was negligibly small (below 5% of a monolayer). Au nanoparticles were grown by evaporating Au wires (purity 99.999% from Alfa Aesar) using an electron bombardment heating (evaporator made by TECTRA). For the preparation of a sample, the flux of Au could be kept constant by controlling the emission current between the W filament and the Au target (from sample to sample, the emission current was varied between 15 and 23 mA to alter the evaporation rate). All STM images were taken using the constant current mode, and PtIr tips were used for imaging the Au nanostructures.

After the STM measurements, some samples were further characterized in a second UHV system equipped with a Cylindrical Hemispherical Analyzer (CHA), an X-ray source, and a He UV lamp. We also prepared Au and Ag nanoparticles on HOPG in the XPS chamber without STM investigations. In this case, the HOPG samples were outgassed at a sample temperature of about 800 K for longer than 12 h. Again, the cleanliness of HOPG was confirmed using XPS. The sputtering conditions in the XPS chamber are quite similar to those in the STM chamber. In the XPS chamber, Au and Ag nanoparticles were grown by resistive heating of W filaments, which wrapped the Au and Ag rods.

3. Results and Discussion

3.1. STM Studies on Au Nanoparticles on Sputtered HOPG. In Figures 1−3, STM images of three different Au/HOPG surfaces with different defect densities and coverages of Au are shown. The defect sites created by sputtering serve as the nucleation centers for metal atoms, and therefore, the sputtering time can be varied to alter the particle density. When

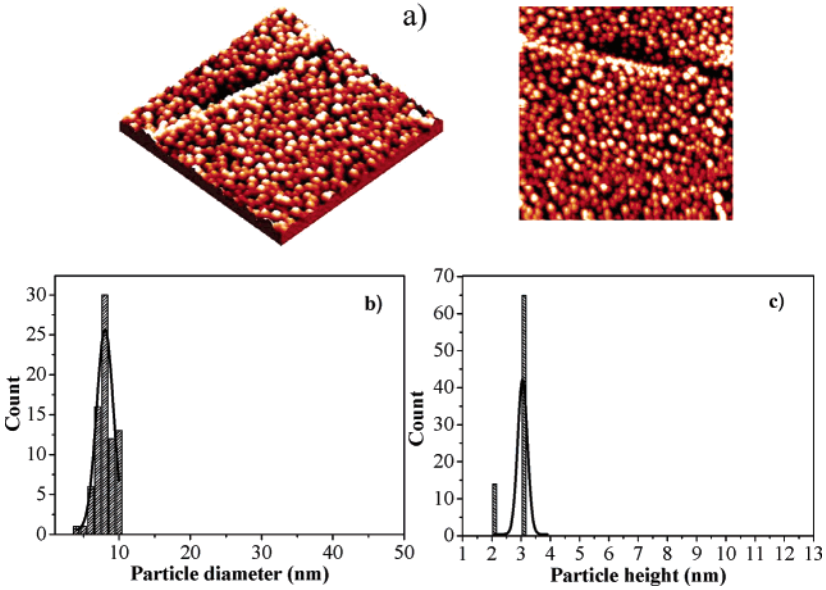

Figure 2. STM data of Au nanoparticles on HOPG. The HOPG sample was sputtered for 5 s (P(Ar) = 5×10^{-5}, 0.5 kV), and Au was evaporated for 5 min with an emission current of 17 mA for evaporating. (a) A 2D and a 3D display of the same image, 256.5 nm × 256.5 nm, tunneling parameter: −1.97 V, 0.08 nA. (b and c) Statistics of the particle diameters and heights.

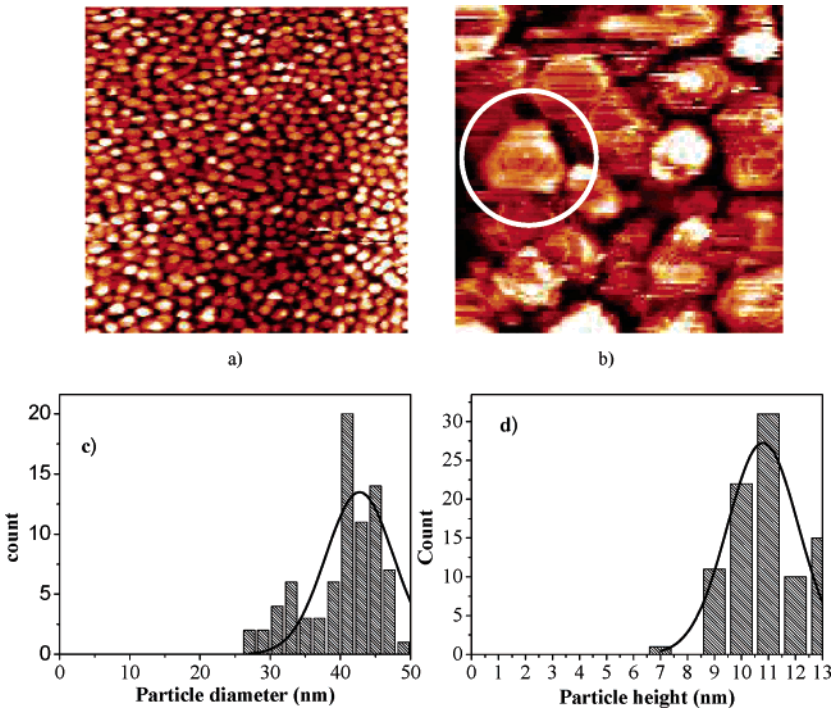

Figure 3. Au nanoparticles on HOPG. The HOPG sample was sputtered for 3 s (P(Ar) = 5×10^{-6} Torr, 0.5 kV), and Au was evaporated for 15 min with an emission current of 22.5 mA for evaporating. (a) Image 996 nm × 1006 nm, tunneling parameter: 4.0 V, 0.22 nA. (b) Parameters: 2.2 V, 0.22 nA, 154 nm × 154 nm. (c and d) Statistics of the particle diameters and heights.

the HOPG surface was sputtered for 10 s at an Ar pressure of 5×10^{-5} Torr, and Au was evaporated for 10 min at an emission current (between target and filament) of 15 mA, Au nanoparticles with a mean diameter of ∼5 nm and height below 2−3 nm could be observed (Figure 1). The particle diameter was determined by measuring the width of the half-maximum of a particle profile.

By decreasing the sputtering time, but increasing the amount of Au atoms deposited on the surface, larger Au particles could be prepared (Figure 2). The defect density was decreased to avoid particles touching each other. The particle diameter increased significantly compared to the sample in Figure 1; however, no significant change in height could be observed. This result may imply that 2D growth dominates in this Au particle size range. However, it should be considered that the height information in Figure 1 can be subject to a relatively large error, since an extremely high sample bias had to be used for taking the image in Figure 1 to ensure a stable imaging. Although the STM resolution is not sufficiently high to accurately identify the particle shape, one can argue that the particles are not completely round-shaped, but facetted. The facet structure becomes much more obvious at higher Au coverages. The particle shapes are also rather similar to those of the Ag nanoparticles on HOPG found in our previous studies.[33]

To further increase the particle size, the defect density was decreased, and a higher Au coverage than that in Figure 2 was

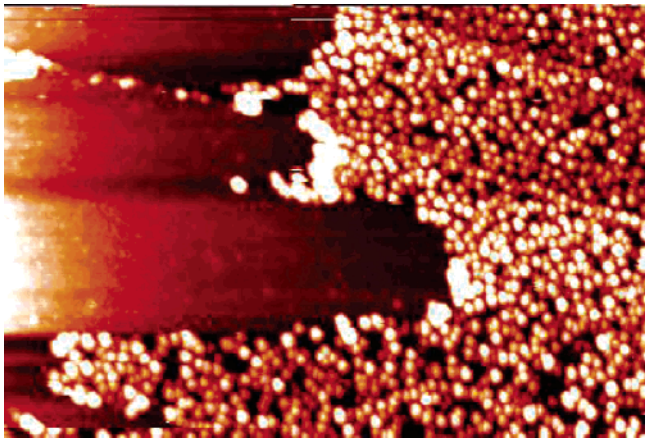

Figure 4. STM images from the same sample as Figure 2, but tip-induced movements of particles can be seen in this figure. Image 495 nm × 335 nm, tunneling parameter: −1.07 V, 0.06 nA.

used (Figure 3). One can observe Au particles of ∼40 nm in diameter and ∼10 nm in height on this sample; that is, both vertical and lateral dimensions increase with particle size. This is in contrast to the growth mode of Au and Ag onWSe_2 surfaces, on which a perfect two-dimensional growth of the particles is preferred, leading to the formation of particles of 2 nm in height and larger than 20 nm in diameter.[34] WSe_2 is also a van der Waals surface like HOPG; however, the particle growth modes on both surfaces are distinctly different.

In the sample in Figure 3, the polyhedral shape (mostly hexagonal) of the particles can be identified, indicating facet formation. Some particles show steps between different planes lying parallel to the surface, instead of forming the ideal truncated octahedral structure (Figure 3b). This result can probably be related to the fact that the metal atoms landed on the topmost terrace of an Au particle cannot diffuse down to the next atomic layer, due to a high Ehrlich−Schwöbel barrier (step edge barrier for the interlayer diffusion), thus, forming an additional plane on top of the terrace.[36−38] When Au was deposited at an elevated temperature of 600 K, the formation of the truncated octahedral particle shape was found previously, implying that room temperature is not sufficient to overcome the activation barrier of the metal atom jumping over the step edges, which becomes possible at elevated temperatures on HOPG.[35] On WSe_2, the ideal truncated octahedron shapes of the Au nanoparticles were observed at room-temperature deposition, whereas the stepped structure could never be identified. This indicates that, even for Au film thicker than 10 atomic layers (2−3 nm), the growth kinetics of the metal film can be influenced by the underlying substrate.[34] The formation of the stepped structures of Au films was studied in detail, which is going to be discussed in section 3.3.

3.2. Tip-Induced Movements of the Particles. For the samples in Figures 1 and 3, different areas of the same samples were imaged with different tips. Similar STM images could reproducibly be obtained from the same samples (data not shown here), implying that we can create homogeneous surfaces in terms of defect density and Au coverage. Different STM images from the one in Figure 2 could be observed, when another area of the same sample was scanned using different tips and tunneling conditions (Figure 4). At the very beginning of the STM measurements in Figure 4, the tip approached the center of the area imaged in Figure 4. A higher tunneling current than that used for the imaging in Figure 2 was set while the tip was approaching the surface. One can see that many Au particles

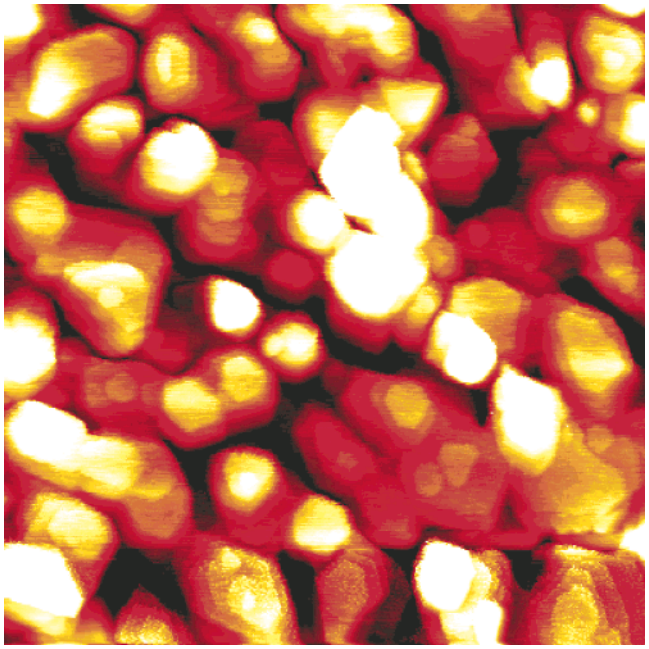

Figure 5. STM image of an Au nanostructured film on HOPG. The HOPG sample was sputtered for ∼5 s (P(Ar) = 5 × 10^{-6} Torr, 0.5 kV), and Au was evaporated for 2 min with an emission current of 22.5 mA for evaporating, 220 nm × 220 nm, tunneling parameter: −1.2 V, 1.3 nA.

are displaced by the STM tips. In the area where the large Au particles are displaced, a number of smaller particles can be observed.

STM samples a much smaller area than XPS, and therefore, tip-induced modifications of the surface structure during STM experiments should yield inconsistent results for the quantitative analysis of XPS and STM images. In our previous studies on Ag nanoparticles on HOPG, the particle densities and sizes in STM images were in good agreement with the quantitative analysis of the XPS data (analysis of the C 1s and Ag 3d peak intensities).[33] For the comparison of STM images and XPS data, one has to take into account that the lateral particle size in STM images can be overestimated by about ∼60%, which has been found in the combined Transmission Electron Microscopy (TEM)/STM studies, and our previous STM/XPS measurements.[32,33] The sample in the STM image in Figure 2 yields an Au(4f)/C(1s) intensity ratio comparable to that of the Ag(3d)/C(1s) of the Ag/HOPG sample with a comparable particle size and density, so that Figure 2 can be considered to be a representative image of the sample.[33] Note that the photoemission cross sections of the Ag 3d and Au 4f differ only by less than 10%.[40]

3.3. Nanostructured Au Films on HOPG. For increased Au coverages, one can observe the formation of nanostructured Au thin films instead of separate particles, as shown in Figure 5. In this case, the existence of steps between different planes becomes more evident than in Figure 3. The formation of the hexagonal plane is again obvious, indicative of the preferred formation of the (111) plane parallel to the surface.

One may argue that the deposition rate of Au was too fast to yield this kind of stepped structures at room temperature. When the deposition rate is too fast, Au atoms can form Au clusters on the topmost terrace of the Au film, before they move down to the next plane. The energy barrier for jumping across a step might be low for an atom; however, the energy barrier for a cluster can be higher, resulting in a film growth, which is

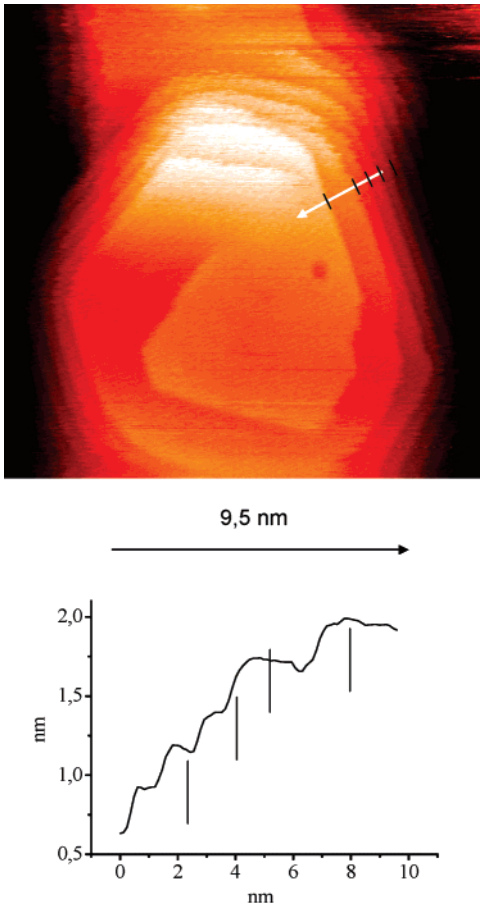

Figure 6. STM image of an Au nanostructured film on HOPG. The HOPG sample was sputtered for ~5 s (P(Ar) = 5 × 10^{-6} Torr, 0.5 kV), and Au was evaporated for 45 min with an emission current of 17 mA for evaporating, 44 nm × 44 nm, tunneling parameter: 1.5 V, 0.3 nA.

strongly limited by the energy barrier for the interlayer diffusion across the steps, as seen in Figures 3 and 5.[41] To study whether the deposition rate of Au influences the particle shape, we deposited an almost equal amount of Au to that in Figure 5, but with a much lower deposition rate (reduced by a factor of ~20−30). As shown in Figure 6, the step structure can still be found, implying that our results are independent of the deposition rate. The profile of the STM image shows that the step height amounts to ~0.2 nm, which corresponds to the size of one atomic layer (Figure 6). For Ag, the diffusion barrier across step-edges has been determined to be 0.06−0.07 eV with a prefactor of 10^{12} s^{-1}, implying that the shapes of particles grown at room temperature and higher temperatures (e.g., 600 K) can be much different.[42]

In general, the sensitivity for determining particle shapes using STM is limited; one often assumes that the particles have ideal forms such as truncated octahedron structures. Our result suggests that the particles can have a much higher defect density than estimated under the assumption of an ideal particle form, since the particle growth is kinetically limited, leaving a higher step density than in an ideal particle shape. Considering that step edges can be active sites of chemical process (heterogeneous catalysis), the exact determination of the number of defect sites of nanoparticles is important.[25] Comparison of the chemical activities of similarly sized Au particles, but of different shapes, is a subject of future studies.

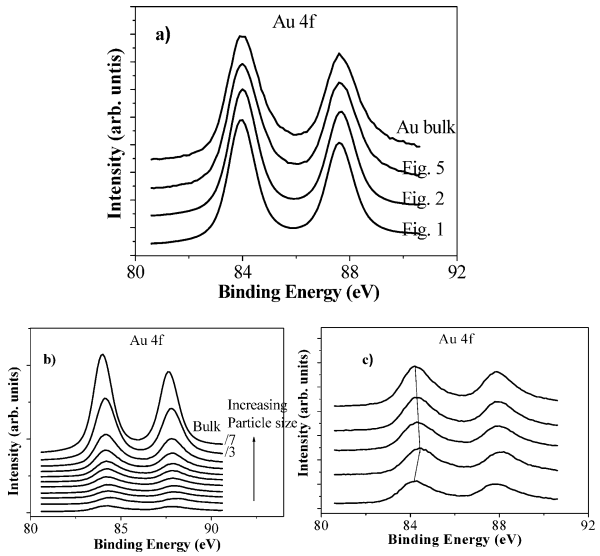

Figure 7. XPS Au 4f level shifts as a function of particle size. (a) Samples studied with STM (Figures 1−5) are transferred and analyzed with XPS. (b and c) The samples were prepared in the XPS chamber. (c) A magnified view of the first four spectra in panel b.

3.4. XPS Studies on Au on HOPG. To shed light on the electronic properties of Au nanoparticles on HOPG, the samples of Figure 1, 2, and 5 were transferred into the STM chamber, and XPS studies on these samples were carried out. As displayed in Figure 7, the Au 4f levels do not show any significant core level shifts, even when the particle size becomes smaller than ~4 nm in lateral size and ~3 nm in height. Only a slight broadening of the Au 4f level can be observed; however, the center of the peak is shifted less than 0.1 eV with respect to the bulk value. We have previously performed combined XPS and STM studies to determine electronic and geometric structures of Ag nanoparticles on HOPG.[33] For similar particle sizes of Ag, positive core level shifts of about 0.5 eV with respect to the bulk value can be observed. Previously, no significant chemical shifts of the Au 4f levels were found for the Au particle on HOPG exceeding 1.5 nm in size, which is in agreement with our data.[24]

To study electronic properties of even smaller structures, Au nanoparticles were prepared on the sputtered HOPG surfaces in the XPS chamber (Figure 7). We have sputtered for much longer time to increase the particle density, which allowed us to detect smaller Au nanoparticles with sufficiently high intensities of the Au 4f peaks. For even smaller Au nanoparticles, first a positive chemical shift of up to ~0.3 eV with respect to the bulk value can be found with decreasing particle size, followed by a negative shift (Figure 7 b,c). This kind of inversion of the core level shifts as a function of particle size has not been found for Ag nanoparticles on HOPG.[33] Previous works on Au nanoparticles on HOPG or amorphous carbons did not yield such an inversion of the Au 4f levels as a function of particle size, which can originate from a different substrate preparation as well as different particle size ranges studied in different groups.[7,23,24] Many of the spectroscopic data were not directly compared to microscopic results of the same samples, and therefore, the particle sizes studied in many previous photoemission studies were not clearly determined. The dissimilar results for Ag and Au nanoparticles suggest that the core level shifts cannot be explained within a simple model, according to which the core level shifts mainly correlate with the efficiency of the screening of the final state of the photoemission, which gradually decreases with decreasing mean

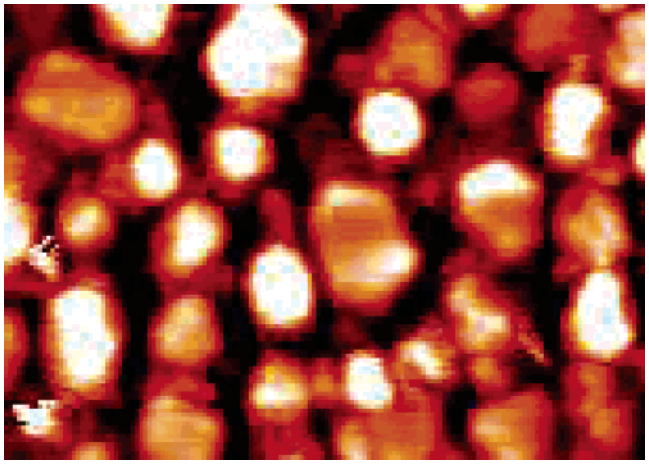

Figure 8. STM images of Ag nanoparticles on HOPG. For relatively flat particles, the formation of the facet structures can be clearly discriminated, 76 nm × 56 nm, tunneling parameter: −5 V, 1nA.

particle diameter. Initial state effects should be taken into account to explain the difference between Ag and Au, which also corroborates the Auger analysis results of the Ag/HOPG system. This will be shown in the next section in detail.

3.5. Comparison of Au with Ag Nanoparticles on HOPG. In our previous studies on Ag/HOPG, the facet formation of Ag nanoparticles was not clearly observed due to the limited lateral resolution of the STM, even though one could recognize that the Ag particles are not completely round-shaped. In a more recent STM image of Ag nanoparticles on HOPG, a hexagonal shape of the particles can be clearly discriminated (Figure 8), implying that the particles preferentially grow along the (111) direction perpendicular to the HOPG surface. The axial ratio of the particles is slightly different between Ag and Au; however, the shapes of Au and Ag nanoparticles seem to be analogous. Note that the hexagonal plane was also observed for larger Au nanoparticles, and for smaller Au nanoparticles, indications for the facet structures could be found. The preference of the growth along the (111) direction could also be shown for Au and Ag on WSe_2.[34] Our observation that there is no significant difference of the particle structure between Ag and Au is in line with the previous results on WSe_2.[34]

As mentioned above, much larger core level shifts for the Ag nanoparticles compared to those of Au on HOPG have been found previously.[33] To shed light onto the origin of the particle size-dependent Ag 3d level shift, Auger analysis was performed. Because of the low intensities of the Auger peaks of Au nanoparticles, the Auger analysis could only be carried out for the Ag systems. It was previously shown by Wagner that the sum of the kinetic energy shift of the Auger peak and the shift of the core level binding energy equals twice the final state contributions of the core level shifts (so-called α-factor).[8,43,44] This suggestion of Wagner can be rationalized, only when the energy shifts of different orbitals are the same. The Auger analysis has been further modified by other groups.[14,45] However, the α-analysis originally suggested by Wagner is still widely used. In particular, on carbon surfaces, it has been previously shown that the Ag 3d, 4d, and Fermi levels shift in a nearly parallel way within a deviation of 0.2 eV, hence, justifying the use of the Auger analysis of Wagner (Figure 10).[6] On alumina surfaces, parallel shifts of the 3d peak and the center of the 4d band of Ag were also found, which were used to demonstrate the validity of the Wagner analysis.[8]

In Figure 9, the Ag 3d spectra and Ag MVV Auger spectra are shown as a function of particle size. Our Auger analysis

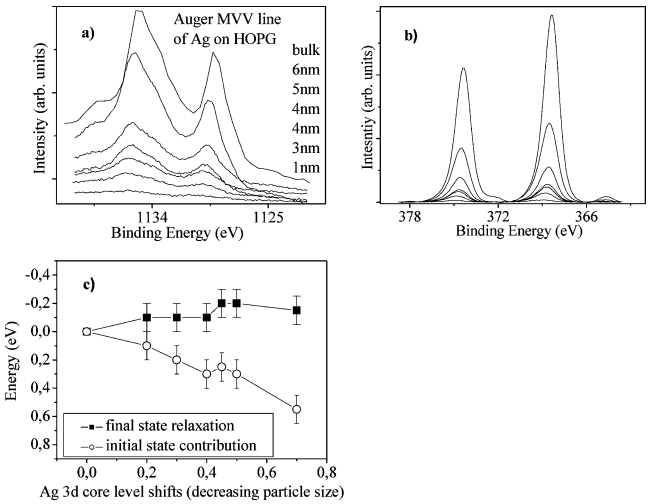

Figure 9. Results of the Auger analysis of the XPS data for Ag on HOPG are demonstrated. Particle sizes were determined from comparison of the XPS data in ref 33, in which combination of XPS and STM was used for the analysis of the Ag/HOPG systems. (a) Auger transition data; (b) Ag 3d core level shifts; (c) results of the Auger analysis. For the XPS data (Ag 3d spectra), each peak was fitted by using two Gaussian functions (a main peak and a shoulder at higher binding energies) to determine the binding energies of the Ag 3d states accurately. The total core level shifts come from $\Delta E - R$, in which E is the initial state contribution and R is the final state relaxation effect.

reveals that the final state effect is about 0.1 eV, independent of the particle size, and the initial state contribution to the positive core level shift significantly increases with decreasing particle size, which is mostly responsible for the positive core level shifts of Ag nanoparticles on HOPG. The fact that the final state effect is less important here compared to other previous studies on nanoparticles on oxide substrates (e.g., alumina) can be explained by the relatively high conductivity of HOPG. Our results are not in line with previous data on Ag on alumina surfaces, in which the chemical shifts were dominated by the final state effects, and the initial state effects were negligibly small (less than 0.1 eV).[8]

For a deeper understanding of the initial state contribution, the following factors should be taken into account:

(1) Metal/support charge transfer: considering that the work function of HOPG (∼4.6 eV) is higher than those of Ag surfaces (∼4.2 eV) by about 0.4 eV, the Ag nanoparticles can be partially positively charged on HOPG, resulting in the positive shifts.[46,47] In contrast, a C to Au charge transfer is expected due to the larger work function of Au (∼5.2 eV).[48] Also, the electron affinities of Au clusters are lower than those of the respective Ag clusters, showing that the Au clusters have much higher propensities to become negatively charged than the Ag clusters.[49] Hence, the larger positive chemical shift of Ag than Au can be explained by the positive and the negative charging of Ag and Au nanoparticles due to the metal/support charge transfer. The parallel shifts of the Ag 3d, 4d, and 5sp as a function of particle size, which have been attributed to the final state effects previously, can also reconcile the formation of positively charged Ag nanoparticles on HOPG. (Actually, the positive shifts of the valence levels tend to be slightly higher than those of the core levels of Ag on HOPG, which can be understood within the charge transfer model.) For Au, an inversion of the core level shifts with decreasing particle size was found for very small particles, also in line with the negative charging of Au nanoparticles. Au nanoparticles show positive core level shifts with respect to the bulk value, and therefore, one cannot say that the negative charging is the only mechanism which explains

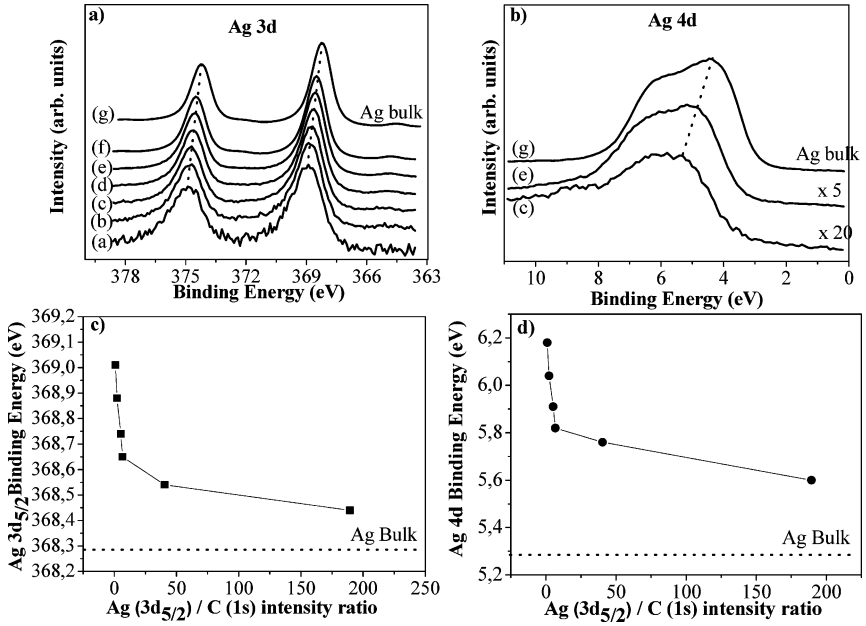

Figure 10. Shifts of the (a) 3d and (b) 4d states of Ag as a function of Ag coverage on sputtered HOPG. (c and d) The changes of the centers of the 3d and 4d states.

the size-dependent changes of the chemical shifts. However, one may suggest that there are other mechanisms common to Ag and Au, which are responsible for the positive core level shifts. Metal/support charge transfer for Ag may results in an additional positive core level shift, whereas the negative charging of the Au nanoparticles partially compensates the positive core level shifts caused by other mechanisms.

(2) Lattice strain: with decreasing particle size, the lattice constant can decrease, which can lead to the rehybridization of the valence d and sp orbitals.[14] This could result in a positive chemical shift of the core levels.[14,25] The lattice strain should be included to fully understand the core level shifts of nanoparticles, yet we suggest that the lattice strain is not the dominating factor to explain the large positive core level shifts of Ag on HOPG. For Ag on carbon, almost parallel shifts of the Ag 3d, 4d, and 5sp levels were observed, which do not rationalize the rehybridization of 4d and 5sp induced by the increased lattice strain for smaller clusters.[6,14] Although we did not measure the Fermi level shifts, our results on Ag 3d and 4d shifts are in agreement with those of Wertheim et al. in ref 6 (Figure 10). It is also important to mention that the sd hybridization of Au clusters is suggested to be stronger than those of Cu and Ag, leading to the formation of planar Au clusters up to the cluster size of ~13.[50] The stronger sd rehybridization of Au clusters should yield a larger positive core level shift of Au than Ag, which is not in agreement with our experimental data.[14,50]

(3) Role of undercoordinated atoms: for a smaller nanoparticle, a higher concentration of undercoordinated atoms exists compared to larger particles and bulk counterpart. Undercoordinated atoms can show different electronic structures than atoms on the perfect surfaces, and therefore, this could lead to the chemical shifts as a function of particle size. Considering that both Ag and Au prefer growth along the (111) direction perpendicular to the surface (inferred by the appearance of the hexagonal shape) according to our STM studies, the geometries of Ag and Au nanoparticles on HOPG are not significantly different. There is no indication that Au or Ag particles on HOPG can show a round shape, as it was found previously for metal particles on other substrates, which may increase the number of undercoordinated atoms significantly.[18] Therefore, we suggest that it is not reasonable to attribute the different core level shifts of Au and Ag nanoparticles on HOPG to the different particle structures.

However, it was previously suggested that a surface Au atom causes a negative core level shift of 0.4 eV with respect to the bulk value, whereas for Ag, a much smaller chemical shift can be found for surface atoms (less than 0.1 eV).[19] One may argue that this could reconcile our experimental observation presented here, since the positive shifts are much less pronounced for Au nanoparticles. The different electronic structures of undercoordinated atoms (band narrowing) yield negative shifts of Au, whereas the same factor has nearly no contribution for the Ag core level shift.

(4) Metal/nonmetal transition: the metal/nonmetal transition of Au and Ag nanoparticles should take place in a similar particles size regime, and therefore, the difference between Au and Ag shown here cannot be considered to be a dominating factor to rationalize the core level shifts of nanoparticles. Also, the metal/nonmetal transition takes place at a particle size of 1−3 nm, which is much smaller than the onset of the core level shifts of Ag.[51,52]

Summarizing, the Auger analysis data of Ag show the importance of the initial state effects in the core level shifts of nanoparticles. Our observation that the Au 4f level first shifts to higher and then to lower binding energies with decreasing particle size suggests that this behavior cannot be explained by a single mechanism. Rather, a combination of various mechanisms should be suggested. Among various origins of the core level shifts by the initial state effects, the lattice strain and metal/nonmetal transition can only partially justify the core level shifts of Ag nanoparticles, since these factors should result in similar core level shifts of Ag and Au, or even larger shifts for Au particles. Together with the final state effects, these factors could be responsible for at most only half of the maximum positive core level shifts of Ag nanoparticles observed in the present work. Metal support interactions and the different electronic structures of the undercoordinated atoms of small particles can justify the different results of Ag and Au. For Ag, a significant positive charging of nanoparticles can explain all our experimental data, namely, the Auger analysis data, core level shifts, and the valence level shifts as a function of particle size.

Considering that the work function of HOPG or amorphous carbon surfaces is higher than Ag, Ag → C charge transfer found in our work might not be surprising. The work function of Au is higher than that of carbon, and therefore, negative charging of Au is expected on HOPG. The Au XPS data are also in line with the negative charging of the Au nanoparticles on HOPG. Dissimilar electronic structures of undercoordinated atoms of nanoparticles compared to the bulk atoms can play a role, but we suggest that the large initial state contribution of the positive core level shifts of Ag nanoparticles can only be rationalized by the charge transfer between carbon and metal.

Recently, Au nanoparticles attracted attention due to their unique chemical activities. Small Au nanoparticles can catalyze many reactions at lower temperatures than other catalysts, whereas larger particles show no reactivities for the same reactions. Oxides are generally used as support materials of Au nanoparticles. Much attention has been paid to the origin of the high reactivities of Au/oxide systems. On one hand, reactions were suggested to take place at the boundary of Au and oxide, in which an oxygen atom of the oxide support can react with other reactants on Au nanoparticles.[53] It was also suggested by different groups that reactions take place on Au nanoparticles, and Au nanoparticles are negatively charged by the support to metal charge transfer.[16,54] We have shown that Au nanoparticles on graphite are most likely negatively charged. The studies on the chemical reactivity of Au/HOPG systems are expected to shed light on the chemical reactivity of negatively charged Au nanoparticles without metal/oxide boundary reactions, since graphite surfaces should have very low oxygen uptake.

4. Conclusions

Using STM, we found that Au nanoparticles on sputtered HOPG can be prepared with a relatively narrow size distribution. For large Au coverages, we could identify the existence of many steps between different planes lying vertical to the surface, which can indicate that the Ehlrich−Schwöbel barrier comes into play for the particle growth at room temperature. Using XPS, we found much smaller core level shifts for Au compared to Ag in the similar particle size range. In particular, the Au 4f level shifts first to the higher binding energy with respect to the bulk value with decreasing particle size, then back to the lower binding energy for even smaller nanoparticles. For Ag, in contrast, only positive shifts of the Ag 3d levels with decreasing particle size were observed. Comparison of Ag and Au on HOPG and the results of the Auger analysis of the Ag/HOPG systems suggest that the Ag and Au particles are positively or negatively charged, respectively, due to the charge transfers between substrates and metal nanoparticles. Our results imply that detailed analysis of XPS data can shed light on the metal support interactions, which can play an important role for, for example, catalysis.

Acknowledgment. We acknowledge the financial support from the Deutsche Forschungsgemeinschaft (DFG) within the program SFB 513 TP A15. We express our gratitude to P. Leiderer and G. Ganteför for fruitful discussions.

References and Notes

(1) Valden, M.; Lai, X.; Goodman, D. W. *Science* **1998**, *281*, 1647−1650.

(2) Haruta, M.; Tsubota, S.; Kobayashi, T.; Kageyama, H.; Genet, M. J.; Delmon, B. *J. Catal.* **1993**, *144*, 175−192.

(3) De Oliveira, L. A.; Wolf, A.; Schüth, F. *Catal. Lett.* **2001**, *73*, 157−160.

(4) Zafeiratos, S.; Kennou, S. *Surf. Sci.* **1999**, *443*, 238−244.

(5) Eberhardt, W.; Fayet, P.; Cox, D. M.; Fu, Z.; Kaldor, A.; Sherwood, R.; Sondericker, D. *Phys. Rev. Lett.* **1990**, *64*, 780−783.

(6) Wertheim, G. K.; DiCenzo, S. B.; Buchanan, D. N. E. *Phys. Rev. B* **1986**, *33*, 5384−5390.

(7) Wetheim, G. K.; DiCenzo, S. B.; Youngquist, S. E. *Phys. Rev. Lett.* **1983**, *51*, 2310−2313.

(8) Luo, K.; Lai, X.; Yi, C.-W.; Davis, K. A.; Gath, K. K.; Goodman, D. W. *J. Phys. Chem. B* **2005**, *109*, 4064−4068.

(9) Engelhoff, W. F., Jr. *Surf. Sci. Rep.* **1987**, *6*, 253−415.

(10) Tanaka, A.; Takeda, Y.; Imamura, M.; Sato, S. *Phys. Rev. B* **2003**, *68*, 195415.

(11) Hövel, K. H.; Grimm, B.; Pollman, M.; Reihl, B. *Eur. Phys. J. D* **1999**, *9*, 595−599.

(12) Hövel, H.; Barke, I.; Boyen, H.-G.; Ziemann, P.; Garnier, M. G.; Oelhafen, P. *Phys. Rev. B* **2004**, *70*, 045424.

(13) Luo, K.; Kim, D. Y.; Goodman, D. W. *J. Mol. Catal. A: Chem.* **2001**, *167*, 191−198.

(14) Richter, B.; Kuhlenbeck, H.; Freund, H.-J.; Bagus, P. S. *Phys. Rev. Lett.* **2004**, *93*, 026805.

(15) Vijayakrishnan, V.; Chainani, A.; Sarma, D. D.; Rao, C. N. R. *J. Phys. Chem.* **1992**, *96*, 8679−8682.

(16) Goodman, D. W. In *Encyclopedia of Nanoscience and Nanotechnology*; Schwarz, J. A., Conlescu, C. I., Putyera, K., Eds.; Marcel Dekker: New York, 2004; pp 611−620.

(17) Howard, A.; Clark, D. N. S.; Mitchell, C. E. J.; Egdell, R. G.; Dhanak, V. R. *Surf. Sci.* **2002**, *518*, 210−224.

(18) Radnik, J.; Mohr, C.; Claus, P. *Phys. Chem. Chem. Phys.* **2003**, *5*, 172−177.

(19) Citrin, P. H.; Wertheim, G. K.; Baer, Y. *Phys. Rev. B* **1983**, *27*, 3160−3175.

(20) Mason, M. G. *Phys. Rev. B* **1983**, *27*, 748−762.

(21) Zhang, P.; Sham, T. K. *Phys. Rev. Lett.* **2003**, *90*, 245502.

(22) Cini, M.; Ce Crescenzi, M.; Patella, F.; Motta, N.; Sastry, M.; Rochet, F.; Pasquali, R.; Balzarotti, A.; Verdozzi, C. *Phys. Rev. B* **1990**, *41*, 5685−5695.

(23) Costanzo, E.; Faraci, G.; Pennisi, A. R.; Ravesi, S.; Terrasi, A.; Margaritondo, G. *Solid State Commun.* **1992**, *81*, 155−158.

(24) Cordes, O.; Harsdirff, M. *Appl. Surf. Sci.* **1988**, *33*, 152−159.

(25) Meyer, R.; Lemire, C.; Shaikhutdinov, S. K.; Freund, H.-J. *Gold Bull. (London)* **2004**, *37*, 72−124.

(26) Sandell, A.; Libuda, J.; Brühlwiler, P. A.; Andersson, S.; Maxwell, A. J.; Bäumer, M.; Martensson, N.; Freund, H. J. *J. Vac. Sci. Technol., A* **1996**, *14*, 1546−1551.

(27) Luo, K.; St. Clari, T. P.; Lai, X.; Goodman, D. W. *J. Phys. Chem. B* **2000**, *104*, 3050−3057.

(28) Rodriguez, J. A.; Kuhn, M.; Hrbek, J. *J. Phys. Chem.* **1996**, *100*, 18240−18248.

(29) Bukhtiyarov, V. I.; Kaichev, V. V. *J. Mol. Catal. A: Chem.* **2000**, *158*, 167−172.

(30) Bukhtiyarov, V. I.; Carley, A. F.; Dollard, L. A.; Roberts, M. W. *Surf. Sci.* **1997**, *381*, L605−L608.

(31) Lim, D. C.; Lopez-Salido, I.; Kim, Y. D. *Surf. Sci.*, submitted for publication, 2005.

(32) Hövel, H.; Becker, Th.; Bettac, A.; Reihl, B.; Tschudy, M.; Williams, E. J. *J. Appl. Phys.* **1997**, *81*, 154−158.

(33) Lopez-Salido, I.; Lim, D. C.; Kim, Y. D. *Surf. Sci.* **2005**, *588*, 6−18.

(34) (a) Rettenberger, A.; Bruker, P.; Metzler, M.; Mugele, F.; Matthes, T. W.; Böhmisch, M.; Boneberg, J.; Friemelt, K.; Leiderer, P. *Surf. Sci.* **1998**, *402*−*404*, 409−412. (b) Zimmermann, J. Ph.D. Thesis, University of Konstanz, 2004.

(35) Irawan, T.; Barke, I.; Hövel, H. *Appl. Phys. A: Mater. Sci. Process.* **2005**, *80*, 929−935.

(36) Schwoebel, R. L.; Shipsey, E. J. *J. Appl. Phys.* **1966**, *37*, 3682−3686.

(37) Erhlich, G.; Hudda, F. G. *J. Chem. Phys.* **1966**, *44*, 1039−1049.

(38) Stegemann, B.; Kaiser, B.; Rademann, K. *New. J. Phys.* **2002**, *4*, 89.1−89.10.

(39) Palmer, R. E.; Pratontep, S.; Boyen, H.-G. *Nat. Mater.* **2003**, *2*, 443−448.

(40) Ertl, G.; Küppers, K. *Low Energy Electrons and Surface Chemistry*; VCH Verlagsgesellschaft: Weinheim, Germany, 1985.

(41) Benz, M.; Tong, X.; Kemper, P.; Lilach, Y.; Kolmakov, A.; Metiu, H.; Bowers, M. T.; Buratto, S. K. *J. Chem. Phys.* **2005**, *122*, 081102.

(42) Caspersen, K. J.; Stoldt, C. R.; Layson, A. R.; Bartelt, M. C.; Thiel, P. A.; Evans, J. W. *Phys. Rev. B* **2001**, *63*, 085401.

(43) Wagner, C. D. *Anal. Chem.* **1972**, *44*, 967−973.

(44) Wagner, C. D. *Anal. Chem.* **1975**, *47*, 1201−1203.

(45) Hohlneicher, G.; Plum, H.; Freund, H.-J. *J. Electron Spectrosc. Relat. Phenom.* **1985**, *37*, 209−224.

(46) Kim, Y. D.; Wei, T.; Wendt, S.; Goodman, D. W. *Langmuir* **2003**, *19*, 7929−7932.

(47) Suzuki, S.; Bower, C.; Watanabe, Y.; Zhou, O. *Appl. Phys. Lett.* **2000**, *76*, 4007−4009.
(48) *Handbook of Chemistry and Physics*, 68th ed.; CRC Press: Boca Raton, FL, 1987.
(49) Taylor, K. J.; Pettiette-Hall, C. L.; Cheshnovsky, O.; Smalley, R. E. *J. Chem. Phys.* **1992**, *96*, 3319−3329.
(50) Häkkinen, H.; Moseler, M.; Landman, U. *Phys. Rev. Lett.* **2002**, *89*, 033401.
(51) Vinod, C. P.; Kulkarni, G. U.; Rao, C. N. R. *Chem. Phys. Lett.* **1998**, *289*, 329−333.
(52) Alvarez, M. M.; Khoury, J. T.; Schaaff, T. G.; Shafigullin, M. N.; Vezmar, I.; Whetten, R. L. *J. Phys. Chem. B* **1997**, *101*, 3706−3712.
(53) Bond, G. C.; Thompson, D. T. *Gold Bull. (London)* **2000**, *33*, 41−51.
(54) Yang, Z.; Goodman, D. W.; Wu, R. *Phys. Rev. B* **2000**, *61*, 14066−14071.